Mechanical and Thermal Forcings of Asian Large-Scale Orography on Spring Cloud Amount and Atmospheric Radiation Budget over East Asia

Li, Jiandong; Geen, Ruth; Mao, Jiangyu; Song, Yajuan; Vallis, Geoffrey K.; Wu, Guoxiong

DOI:
10.1175/JCLI-D-22-0797.1

Mechanical and thermal forcings of Asian large-scale orography on spring cloud amount and atmospheric radiation budget over East Asia

Jiandong Li[1], Ruth Geen[2], Jiangyu Mao[1], Yajuan Song[3], Geoffrey K. Vallis[4], and Guoxiong Wu[1]

[1]State Key Laboratory of Numerical Modeling for Atmospheric Sciences and Geophysical Fluid Dynamics, Institute of Atmospheric Physics, Chinese Academy of Sciences, Beijing, China

[2]Earth and Environmental Sciences, University of Birmingham, Birmingham, UK

[3]First Institute of Oceanography, Ministry of Natural Resources, Qingdao, China

[4]Department College of Engineering, Mathematics and Physical Sciences, University of Exeter, Exeter, UK

Submitted to

Journal of Climate

February 2023

Corresponding author: Jiandong Li, lijd@mail.iap.ac.cn

ABSTRACT:

Asian large-scale orography profoundly influences circulation in the North Hemisphere. Considerable spring top-of-the-atmosphere (TOA) radiative cooling over Southeast China (SEC) is very likely related to upstream orography forcing. Here we investigate the mechanical and thermal forcings of Asian large-scale orography, particularly the Tibetan Plateau (TP), on downstream East Asian cloud amount and atmospheric radiation budget during March-April using the Global Monsoons Model Intercomparison Project simulations. The thermal forcing drives significant surface heating and a low-level cyclone over the TP, pumping low-level air to the middle troposphere. Ascent and water vapor convergence triggered by the thermal forcing favor air condensation, low-middle clouds, and resultant strong spring cloud radiative cooling over SEC. Moreover, the thermal forcing moves the position of cloud radiative cooling westward towards the TP. The TP's blocking role weakens low-level westerlies over SEC, but its deflecting role increases downstream high-level westerlies, dynamically favoring cloud formation over SEC and the eastward ocean. In addition, the TP can force ascent and increase cloud amounts over the western and central TP. The thermal forcing contributes to 57.1% of total cloud amount and 47.6% of TOA cloud radiative cooling induced by the combined orography forcing over SEC while the mechanical one accounts for 79.4% and 95.8% of the counterparts over the ocean to the east of SEC. Our results indicate that Asian large-scale orography shapes the contemporary geographical distribution of spring East Asian cloud amount and atmospheric radiation budget to a large extent.

KEY WORDS: Large-scale orography forcing, Tibetan Plateau, Southeast China, cloud amount, atmospheric radiation budget

SIGNIFICANCE STATEMENT:

Clouds tied to large-scale topography and circulation exhibit some remarkable geographical distributions. The global strongest cloud radiative cooling, with an intensity of up to -90 W m^{-2}, occurs over Southeast China (SEC) during March-April.

The primary purpose of this study is to understand the influences of Asian large-scale orography, particularly the Tibetan Plateau (TP), on this unique climatic phenomenon using the latest climate model simulations. Our results show that Asian large-scale orography forcing significantly increases ascent, low-middle cloud formation, and resultant strong spring cloud radiative cooling over SEC and downstream ocean. The sensible-heat-driven air pump induced by the TP's thermal forcing maintains strong cloud radiative cooling over SEC. This study provides valuable insights that link Asian large-scale orography forcing to downstream cloud-radiation characteristics.

1. Introduction

Clouds strongly modulate the global energy balance via their shortwave reflecting, longwave trapping, and radiative heating in the atmosphere (Allan, 2011; Li et al., 2015; Loeb et al., 2018; Wild, 2020; Forster et al., 2021). In recent decades, the cloud-radiation process continues to be one of the key influencing factors and uncertainties for climate simulation and future projection under global warming (Cess et al., 1990; Stephens, 2005; Bony et al., 2015; Zelinka et al., 2020). At the regional scale, cloud amount and cloud radiative effects tied to large-scale topography and circulation exhibit remarkable geographical distribution. Notably, large amounts of low-middle clouds accompanied by the global strongest cloud radiative cooling at the top of the atmosphere (TOA) in spring, with an intensity of up to -90 W m^{-2} (Fig. 1a), occur over Southeast China (SEC) located downstream of the Tibetan Plateau (TP) (Klein and Hartmann, 1993; Zhang et al., 2013; Li et al., 2017, 2019). This distinctive cloud radiative cooling over SEC stably maintained in March-April can regulate atmospheric radiation budget and surface temperature (Yu et al., 2004; Guo et al., 2015; Li et al., 2021). Spring is a crucial transition season for the East Asian climate and agriculture. The onset and migration of East Asian subtropical monsoon highly rely on spring atmospheric thermal states that are closely related to atmospheric diabatic heating and radiation budget (Ding and Chan, 2005; Yanai and Wu, 2006; Zhao et al., 2007; He et al., 2008). Thus, distinctive spring cloud amount and radiative cooling over SEC very likely play a vital role in the East Asian subtropical monsoon process. Hence, it is essential to reveal the primary climatic factors that dominate East Asian cloud and atmospheric radiation budget in spring.

Numerous studies pointed out that the East Asian climate is profoundly influenced by the mechanical and thermal forcings of Asian large-scale orography, especially the TP (Yanai et al., 1992; Kitoh, 2004; Wu et al., 2015; Duan et al., 2020). The TP covers an area of about 2.5 million square kilometers with an average altitude of over 4000 m (You et al., 2021). In spring, the TP's detouring role and the cyclonic low pressure caused by the sensible heating over the Southeast TP can force low-level southerly wind and water vapor to converge in its downstream region, favoring persistent precipitation and cloud amount over SEC (Wan and Wu, 2007; Li et al., 2019). The dynamic drag and thermal advection of the TP cause the low-level convergence, mid-level divergence, and resulting ascending motion over eastern China in late winter and early spring (Yu et al., 2004; Li and Gu, 2006; Wu and Chou, 2013; Zhang et al., 2013). Moreover, the TP can modulate the position of a high-level westerly jet, and the interplay between low-level and high-level TP's dynamic roles can affect the existence of spring precipitation and its subsequent northward propagation (Molnar et al., 2010; Chiang et al., 2020). On geologic timescales, previous studies have argued that the TP's mechanical and thermal forcings arising from its significant topography shape the contemporary geographical distribution of summer East Asian monsoon circulation and rainfall to a large extent (Wu et al., 2007; Boos and Kuang, 2010). Some ancient Chinese literature reported perennial mountain clouds over SEC. For example, a famous allusion is that dogs often bark once the sun comes out in South Sichuan of SEC where strong sunshine is rare (Liu, 813). Given the strong linkage between the TP's forcing and its downstream East Asian circulation, it is very likely that clouds and the resultant atmospheric radiation budget over East Asia that are sensitive to regional circulation are also susceptible to the large-scale orography forcings mentioned above.

Many studies have examined the impacts of Asian large-scale orography on East Asian circulation and precipitation (e. g. Flohn,1957; Ye et al., 1959; Wu et al., 2007; Duan et al., 2011; He et al., 2019; Chiang et al. 2020). However, the climatic behaviors of spring clouds differ from precipitation in term of the spatial distribution, intensity, and lifetime over East Asia (Li and Yu, 2014; Li et al., 2019). It remains unclear how the mechanical and thermal forcings of Asian large-scale orography influence the generation of springtime cloud amount and atmospheric radiation budget over East Asia, especially for SEC. The answers to these issues are promising to provide new insights into the climatic mechanisms of East Asian cloud-radiation characteristics mentioned above. The difficulties of the previous study lie in the mechanical and thermal effects of Asian large-scale orography mixed in the current topography state. We can't identify their separate roles with observational analysis alone. Recently, the climate model simulations from the Global Monsoon Model Comparison Plan (GMMIP) in the Coupled Model Intercomparison Project Phase 6 (CMIP6) were released (Eyring et al., 2016; Zhou et al., 2016). Orography sensitivity experiments in GMMIP have proved valuable in distinguishing the roles of Asian large-scale orography's mechanical and thermal forcings on the precipitation over Asian monsoon and arid regions (e.g. Sun and Liu, 2021; Luo et al., 2022).

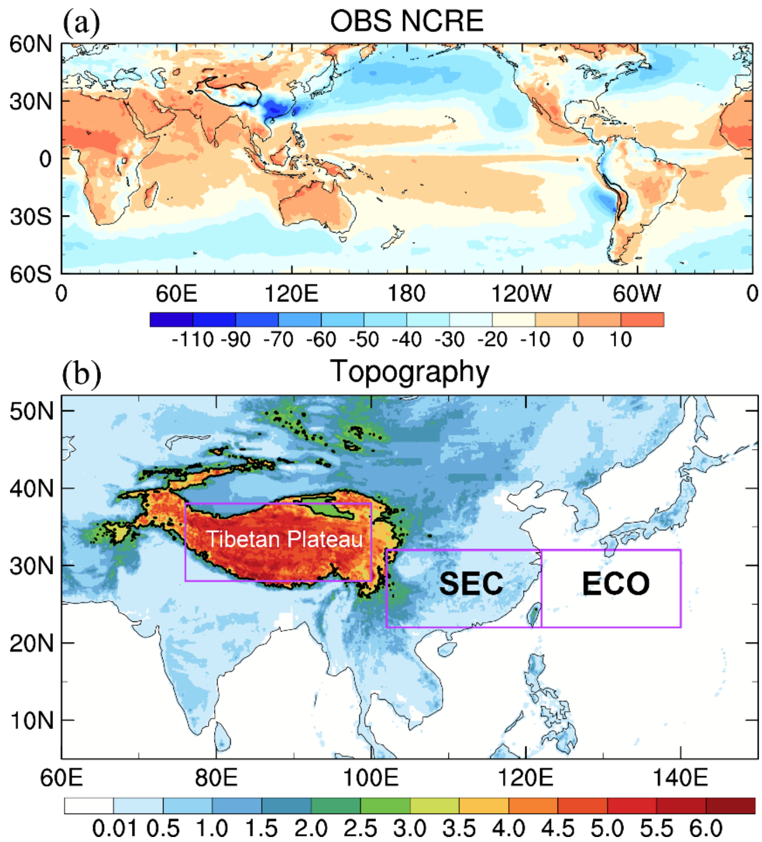

FIG. 1. (a) March-April mean net cloud radiative effect (NCRE: W m^{-2}) from CERES-EBAF satellite data during 2001-2014; (b) Topography (km) of Asian large-scale orography and the study regions. Dark orchid rectangles indicate Southeast China (SEC; 22–32°N, 102–122° E), the ocean to the east of Southeast China (ECO; 22–32 °N, 122–140° E), and the Tibetan Plateau (TP; 28–38° N, 76–100° E). The solid black line denotes the TP's boundary over 3000m.

This study uses two terrain sensitivity experiments from the GMMIP to investigate how Asian large-scale orography forcing affects cloud amount and atmospheric radiation budget over its downstream East Asian regions, emphasizing SEC. This paper is organized as follows. Section 2 introduces the data and methods. Section 3 evaluates the simulation performances of the climate model used in this study. Section 4 shows the major impacts of the mechanical and thermal forcings of Asian large-scale orography on cloud amount and atmospheric radiation budget over East Asia. Section 5 examines the influencing mechanisms for the above impacts through the relationship between changes in dynamical and thermal conditions and cloud amounts mainly arising from the TP's forcings. Section 6 summarizes the main conclusions of this study and gives a brief discussion.

2. Data and Method

a. Data

The monthly outputs from the GMMIP Tier-1 and Tier-3 experiments are used in this study. Tier-1 is the standard Atmospheric Model Intercomparison Project (AMIP) experiment that runs with CMIP6 natural and anthropogenic historical forcings and observational sea surface temperature during 1870–2014 (Eyring et al., 2016; Zhou et al., 2016). Tier-1 is approximately historical climate and is used as the control experiment (hereafter Exp. CTL). We additionally use two orographic sensitivity experiments from Tier-3 covering 1979-2014. The first reduces large Asian orography, including the Tibetan-Iranian-Plateau, to 500m (hereafter Exp. TIP), with other surface properties unchanged. The second keeps modern orography but turns off the sensible heat at elevations above 500 m by setting the vertical temperature diffusion term to zero in the atmospheric thermodynamic equation at the bottom boundary layer (hereafter Exp. TIP_nosh). Other model configurations in TIP and TIP_nosh are identical to CTL. More details about the model experiments can be found in Zhou et al. (2016). Two climate models in GMMIP Tier-1 conducted these three experiments, and one model is the First Institute of Oceanography-Earth System Model version 2 (FIO-ESM-2-0) (Qiao et al., 2013; Song et al., 2020), with a horizontal resolution (0.9° latitude × 1.25° longitude) and 30 vertical layers. FIO-ESM-2-0 outputs complete radiation fluxes and three-dimensional cloud amounts and cloud water content that are needed to examine cloud amounts and atmospheric radiation budget. FIO-ESM-2-0 can reproduce major global climatic features, including the Asian monsoon circulations and precipitation

(Ying et al., 2020). This study therefore chooses the simulations from FIO-ESM-2-0 model.

To evaluate the performance of FIO-ESM-2-0 in the cloud-radiation characteristics, we utilize monthly radiation data from the CERES-EBAF Ed4.1 product since 2000 (Loeb et al., 2018). CERES-EBAF gridded at a spatial resolution of 1°×1° is the most reliable dataset for TOA and surface radiative fluxes, which are widely used as observations to evaluate the Earth's radiation balance and cloud roles (Wild et al., 2020; Forster et al., 2021). ERA5 reanalyzed data (Hersbach et al., 2020) since 2001 are used to assess the skill of the simulated meteorological fields.

b. Model experiments and analysis method

In this study, the thermal, mechanical, and combined forcings of Asian large-scale orography are defined as CTL minus TIP_nosh, TIP_nosh minus TIP, and CTL minus TIP, respectively. This method of separating thermal and mechanical forcings was also used in previous studies (Boos and Kuang 2010, 2013; Wu et al. 2007, 2012; Sun and Liu, 2021). Note that the TP includes most areas above 3000 m in CTL and TIP_nosh runs, implying the TP's mechanical forcing may have a central role in local dynamical response over East Asia. In addition to the TIP, the Mongolia, Loess, and Yungui plateaus covering large areas with elevations over 500 m can somewhat pose a thermal forcing on regional circulation. The three model runs are driven by observational sea surface temperature, and the interaction between air and sea is excluded. In this context, the simulated circulation changes arise mainly from the atmospheric and land processes associated with Asian large-scale orography.

This study focuses on the changes in the spatial distribution and intensity of cloud amount and water content as critical cloud properties. We measure atmospheric radiation budget through the TOA net radiative flux (R_T) and cloud radiative effects (CREs) that are strongly regulated by cloud amount. The R_T and CREs can represent the Earth's energy budget and climate sensitivities caused by natural and anthropogenic forcings (Kiehl and Trenberth, 1997; Flato et al., 2013; Wild et al., 2014, 2020). The R_T is the difference between absorbed shortwave radiation (ASR) and outgoing longwave radiation (OLR) at the TOA (Fasullo and Trenberth, 2008). CREs are calculated from the difference in radiative fluxes between clear-sky and all-sky radiative fluxes for the TOA, atmosphere, and surface (Ramanathan, 1987; Allan, 2011). The formulas of CREs are listed in the Appendices. We focus on TOA and atmospheric CREs, including longwave, shortwave, and net items, and hereafter they are abbreviated as LWCRE, SWCRE, and NCRE at the TOA and $LWCRE_A$, $SWCRE_A$, and $NCRE_A$ in the atmosphere. Other abbreviations are listed in Table A1. The signs of SWCRE and NCRE are usually negative, and their decrease in absolute values denotes the decrease in cloud radiative cooling at the TOA.

March-April is selected as the spring period when the TP's thermal and mechanical forcings coexist and regional NCRE is the strongest over SEC (Fig. 1a). Besides, the circulation pattern and cloud distribution are stable in eastern Asia continents and surrounding ocean regions in March-April. In contrast, May is not a typical spring period over SEC. Summer monsoon rain usually breaks over the South China Sea and SEC in late May when circulation conditions exhibit abrupt variations relative to early May (Ding and Chan, 2005; He et al., 2008). Observational and simulated data during 2001-2014 are extracted to evaluate FIO-ESM-2-0 simulations. The 30-yrs data in three orography experiments during 1985-2014 are selected to examine Asian large-scale orography. Based on the position of East Asian cloud regime and large-scale orography, this study selects three study domains, including SEC (104-122°E and 22-32°N), the TP (76-102°E and 28-38°N), and the ocean to the east of Southeast China (ECO: 122-140°E and 22-32°N) (Fig. 1b). SEC is our emphasized region, and other two are as comparison regions.

3. Model evaluation

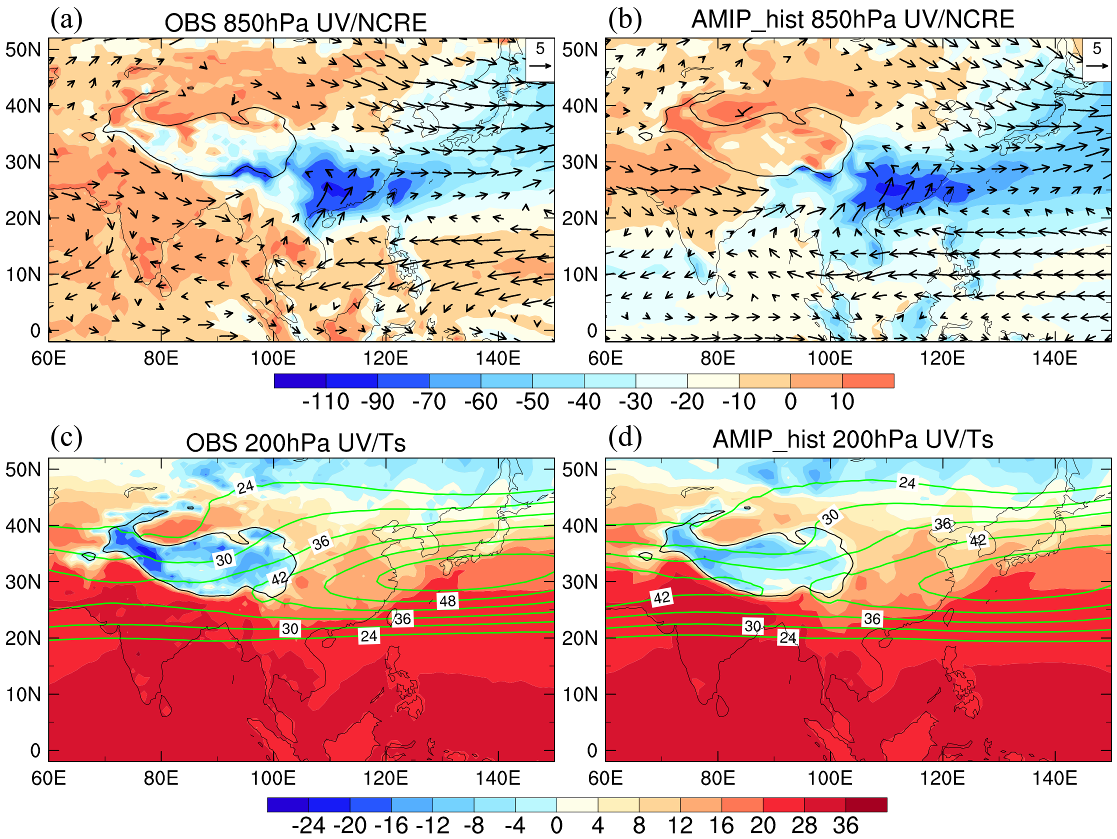

FIG. 2. March-April mean (a) observational 850-hPa horizontal wind (vector; m s^{-1}) from ERA5 reanalysis (Hersbach et al., 2020) and NCRE (shading; W m^{-2}) from CERES-EBAF satellite data (Loeb et al., 2018) and (b) simulated counterparts in AMIP_hist run; (c) observational 200-hPa horizontal wind speed (contour; m s^{-1}) and surface temperature (shading; Ts, ℃) from ERA5 reanalysis and (d) simulated counterparts in AMIP_hist run. Here, the period is 2001-2014. The solid black line denotes the TP's boundary over 3000m. The 850-hPa wind is masked when the grid surface pressure is less than 850 hPa.

At the beginning of this study, it is necessary to evaluate the model performance in clouds and circulation in March-April to verify FIO-ESM-2-0 model results. Here we select NCRE calculated from CERES-EBAF surface temperature (Ts), low-, and high-level wind fields from ERA5 reanalysis during 2001-2014 as key assessment variables tightly connected with the regional cloud-radiation process. In the observation, strong NCRE occurs in the south flank of the TP and SEC, with the maximum intensity up to −90 W m^{-2}. The large magnitude of NCRE extends to the eastern ocean adjacent to SEC (Fig. 2a). A low-level westerly detouring wind is located south of the TP. A low-level anticyclone appears over the northwestern Pacific, along the west side of which the southerly wind comes to SEC (Figs. 2a,b). Meanwhile, northern detouring currents appear in the northern TP, north China, and Japan (Figs. 2a.b). In addition, the subtropical 200-hPa westerly jet passes south of the TP. The jet axis appears over the north of SEC, causing a pumping role in the low-middle atmosphere (Fig. 2c). High-level westerly jet is critical to East Asian climate (Liang and Wang, 1998). These low- and high-level circulation conditions in March-April are closely related to the TP's forcing (Kitoh, 2004; Wu et al., 2007), and they favor water vapor convergence, updraft, and cloud formation over SEC and its eastern coasts (Zhang et al., 2013; Li et al., 2019).

The FIO-ESM-2-0 model can reproduce the spatial pattern of NCRE, including its central location and intensity over SEC, corresponding to well-simulated circulation and Ts over Asian continents and adjacent oceans (Figs. 2b,d). The simulated domain-mean NCRE over SEC is −66.0 W m^{-2}, comparable to the observational counterpart (−63.9 W m^{-2}). Simulated NCRE magnitude (cooling effect) is stronger between the North Indian Ocean and western Pacific and weaker over the eastern TP compared with the observation (Fig. 2b). As for atmospheric models in CMIP6 GMMIP Tier-1 experiments, three models (CESM2, FIO-ESM-2-0, and TaiESM1) show high capabilities in reproducing March-April mean NCRE and circulation over East Asia. The position and intensity of NCRE, 850-hPa wind, 500-hPa ascending, and 200-hPa westerly are well captured in these three models (Figs. S1-S2). It is worth noting that FIO-ESM-2-0 and TaiESM1 belong to the Community Earth System Model (CESM) family of models and have similar atmospheric parameterizations to those in CESM (Hurrell et al., 2013; Ying et al., 2020; Wang et al., 2021). Recent work has pointed out that CESM2 model better simulates the climatological mean state of the circulation and relevant TOA cloud-radiation characteristics over Asian monsoon regions relative to most CMIP6 models (Li et al., 2021; Yu et al., 2022). Thus, the good model reproducibility of FIO-ESM-2-0 in key cloud radiative effects and circulation over the Asian region ensures that the following model experiments can provide confident results for our study targets.

4. Simulated cloud amount and atmospheric radiation budget

This section first presents climatological March-April mean simulations from 1985-

2014 from three GMMIP experiments. We compare these results and then identify possible impacts of Asian large-scale orography on cloud amount and atmospheric radiation budget over East Asia, especially SEC. Atmospheric radiation budget focuses on radiation fluxes and CREs at the TOA and atmospheric radiative cooling (heating) role due to clouds.

a. Geographical distribution of cloud-radiation variables and circulation

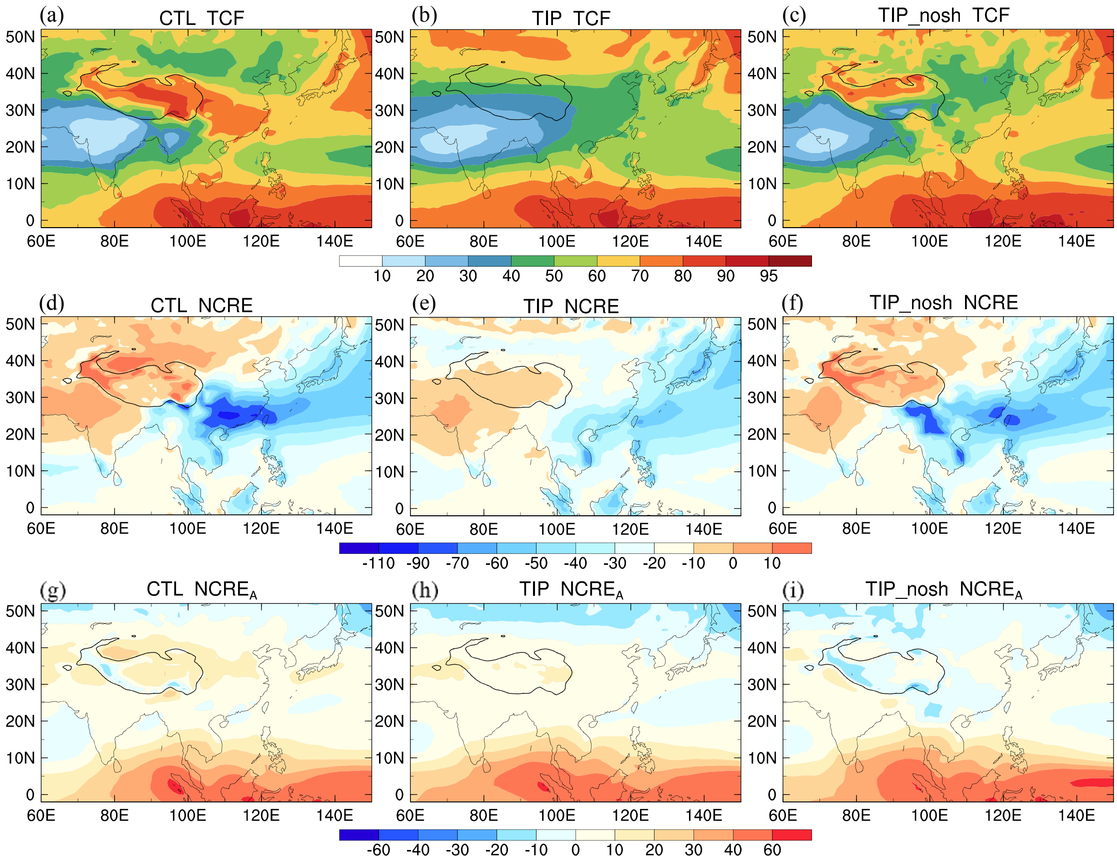

FIG. 3. March-April mean total cloud fraction (TCF; %) in (a) CTL, (b) TIP, and (c) TIP_nosh runs during 1985-2014. (d)-(f) are NCRE at the TOA (W m^{-2}) in these three runs. (g)-(i) are $NCRE_A$ in the atmosphere (W m^{-2}) in these three runs. The solid black line denotes the TP's boundary over 3000m.

Figure 3 shows the geographical distribution of cloud amount and CREs in three experiments, and Figure 4 gives TOA radiation budget. To compare regional differences, Table 1 lists cloud-radiation variables averaged over SEC, the TP, and ECO. In the control experiment, large amounts of cloud fractions (>70%) occur over the TP, SEC, and tropical region (Fig. 3a), corresponding to apparent ascending motion (Fig. S3g). In contrast, less cloud amount (<40%) appears over the Arabian sea, Indian continents, and the Bay of Bengal (Fig. 3a), with evident descent (Fig. S3g). Strong cloud radiative cooling occurs over the south flank of the TP, SEC, and East China Sea, with a cooling center in SEC (Fig. 3a). The domain-mean NCRE over SEC is −66.3 W m^{-2} dominated by SWCRE (−93.7 W m^{-2}) (Table 1). In the meantime, the R_T magnitude over SEC is weaker relative to surrounding areas, and its peak center is even up to −20.0 W m^{-2} (Fig. 4a), which is caused by the strong cloud reflecting role. Figures 5 and S4 show the vertical distribution of cloud amount and cloud water content in three experiments. Most cloud amounts and cloud water content over SEC are mainly distributed below 500-hPa, and the air temperature in large value areas of these cloud amounts (water content) is higher than zero centigrade (Figs. 5a and S4a). Considerable amounts of high clouds with a peak occurring between 200-300 hPa level over SEC, but these high clouds have lower water content than low-level clouds (Figs. 5d and S4d). This implies that low-level clouds over SEC mainly consist of liquid or supercooled cloud water in March-April, which can strongly reflect shortwave radiation and cause a large radiative cooling role (Hu et al., 2010; Matus and L'Ecuyer, 2017; Li et al., 2019). This distinctive TOA radiative cooling over SEC relates to the favorable circulation conditions mentioned above (Figs. 2a,b and S3g). Note that despite the substantial cloud amount over the TP and tropical regions, the significant cancellation between LWCRE and SWCRE allows regional NCRE to be a smaller intensity (Fig. S5a). As listed in Table 1, LWCRE and SWCRE are 39.8 and −41.5 W m^{-2} averaged over the TP, respectively, causing a weak NCRE (−1.7 W m^{-2}). Cloud radiative heating in the atmosphere that relates to high clouds occurs over the TP, North China, and tropical regions (Figs. 3g and 5a). Meanwhile, cloud longwave radiative cooling in the atmosphere appears over SEC, where large amounts of low clouds block downward longwave radiation (Fig. S6d). Another noticeable point is the much lower OLR over the TP relative to surrounding and tropical ocean regions (Fig. 4g), which arises from the high TP elevation.

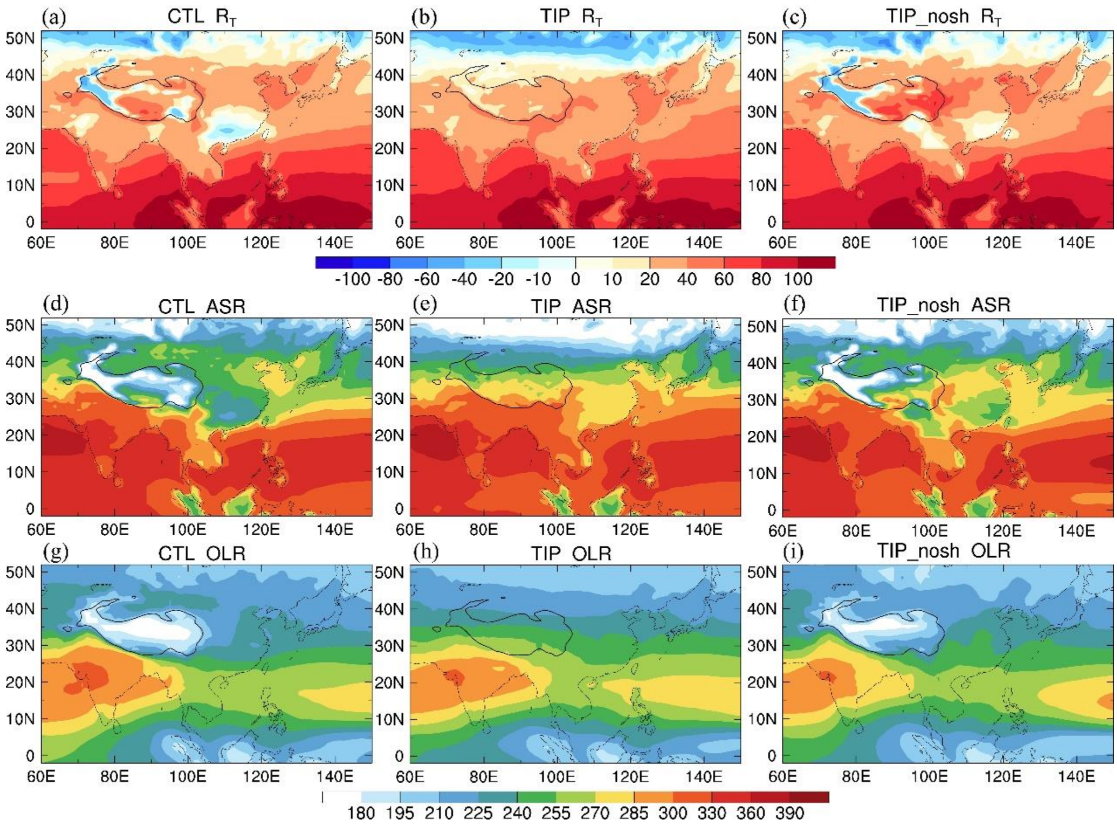

FIG. 4. March-April mean TOA radiation budget (R_T; W m^{-2}) in (a) CTL, (b) TIP, and (c) TIP_nosh runs during 1985-2014. (d)-(f) are absorbed shortwave radiation at the TOA (ASR; W m^{-2}) in these three runs. (g)-(i) are outgoing longwave radiation at the TOA (OLR; W m^{-2}) in these three runs. The solid black line denotes the TP's boundary over 3000m.

When the TP surface sensible heat is removed in TIP_nosh run, cloud fractions over the southeast TP and SEC markedly decrease (Figs. 3c and 5c). In contrast, cloud fractions change little over other subtropical regions, such as South Asia and Western North Pacific (Fig. 3c). Over SEC, strong cloud radiative cooling at the TOA weakens in TIP_nosh, and its cooling center moves eastward relative to the control run (Figs. 3f and S5c). The cloud heating role in the atmosphere also decreases due to less low clouds and resultant cloud atmospheric shortwave heating relative to CTL run (Figs. 3g,i and S6a,c). Meanwhile, the magnitude of ASR and OLR increase over the eastern TP and SEC, leading to a weak positive R_T over SEC (Figs. 4c,f,i). When Asian large-scale orography is reduced to 500 in TIP run, cloud amount over the TP, SEC, and ECO and robust TOA cloud radiative cooling over SEC substantially decrease compared with the control run (Figs. 3b,e, 5b, and S5b). In TIP run, clouds exert a heating role in the atmosphere over the TP and SEC but a cooling role over ECO (Fig. 3h). The westerly wind prevails at mid-latitudes from the TP to Southern Japan, accompanied by the descending motion (Figs. S3b,h). Compared with the other two runs, the low-level southwesterly wind imported from the Bay of Bengal into SEC almost disappears while the southerly from South China Sea remains in TIP run (Fig. S3h). Although the high TP is removed in TIP run, the remaining land-sea distribution can provide an essential land-sea thermal contrast over East Asia in spring (Rodwell and Hoskins, 2001). A low-level southerly is induced, and water vapor is fed into SEC along the western Pacific subtropical anticyclone (Figs. S3e,h). Thus, certain amounts of cloud fractions and NCRE appear over SEC (Figs. 3b,e). Notably, the magnitude of OLR and R_T over the TP and surrounding regions are much enhanced with the disappearance of their high orography (Figs. 4b,h), which relates to enhanced surface temperature due to reduced elevation.

TABLE 1. March-April mean cloud-radiation variables in CTL run averaged over Southeast China (SEC: 22-32°N, 102-122°E), the ocean to the east of SEC (ECO: 22-32°N, 122-140°E), and the Tibetan Plateau (TP: 28-38°N, 76-100°E; >3000m) during 1985-2014.

	SEC	ECO	TP
TOA			
RSDT	404.3	404.4	386.1
RSUT	157.4	123.8	136.6
ASR	246.9	280.6	208.0
R_T	8.8	33.4	22.0
RSUTCS	63.8	42.5	386.1
SWCRE	-93.7	-81.3	-41.5
OLR	238.1	247.2	186.0
OLRCS	265.4	271.8	225.8
LWCRE	27.3	24.6	39.8
NCRE	-66.3	-56.7	-1.7
TCF	69.9%	66.0%	71.8%
Atmosphere			
Absorbed shortwave radiation	107.7	96.5	66.7
Clear-sky absorbed shortwave radiation	97.1	87.1	53.1
$SWCRE_A$	10.6	9.3	13.7

Net longwave radiation	-194.4	-192.9	-112.9
Clear-sky net longwave radiation	-188.2	-187.1	-106.6
$LWCRE_A$	-6.2	-5.8	-6.3
$NCRE_A$	4.4	3.5	7.3

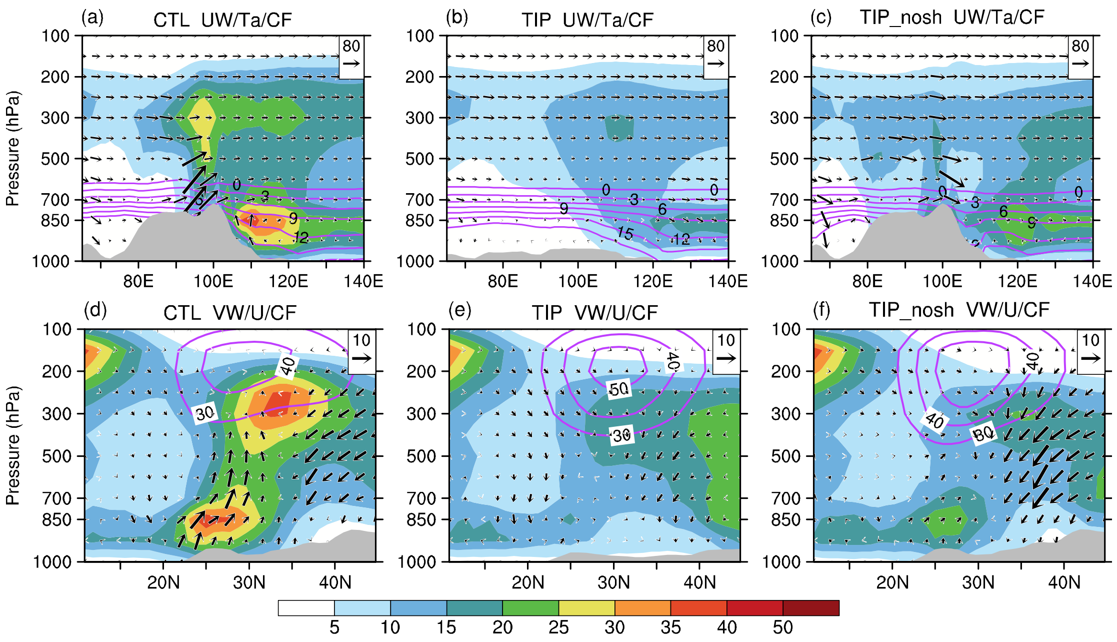

FIG. 5. March-April mean pressure-longitude cross section of cloud fraction (shading; CF: %), air temperature (contour; Ta: °C), and wind circulations (vector; vertical wind (multiplied by 1000) in Pa s^{-1} and zonal wind in m s^{-1}) in (a) CTL, (b) TIP, and (c) TIP_nosh runs averaged over 22-32°N. (d)-(f) are for pressure-latitude cross section of CF (shading; %), zonal wind (contour; m s^{-1}), and wind circulations (vector; vertical wind (multiplied by 200) in Pa s^{-1} and meridional wind (multiplied by 0.05) in m s^{-1}) averaged over 104-122°E. Here, the period is 1985-2014 and the gray shading is the orography altitude.

b. Changes in cloud amount and atmospheric radiation budget induced by Asian large-scale orography

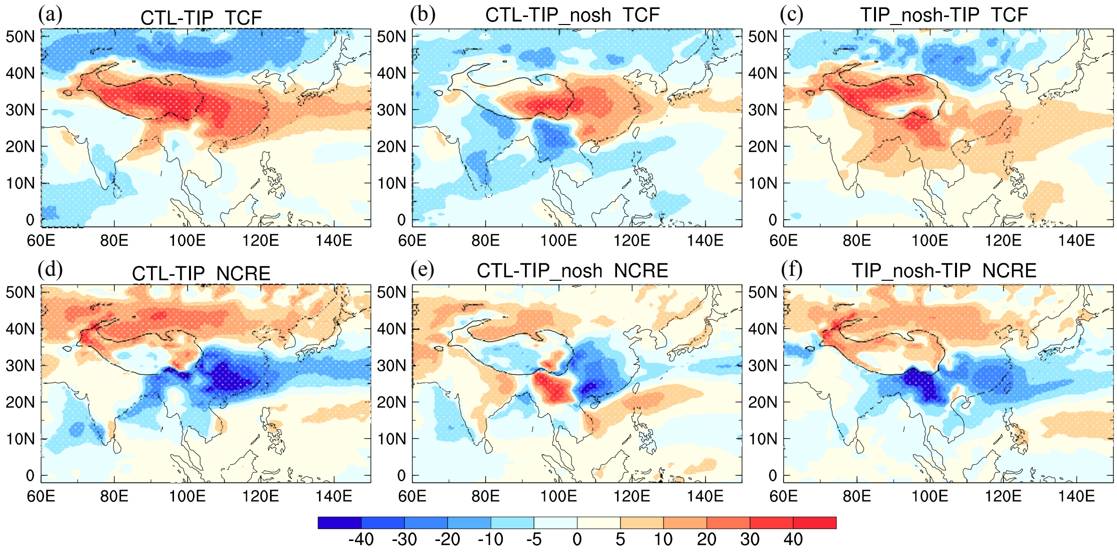

FIG. 6. March-April mean TCF (%) for the difference of (a) CTL and TIP experiments, (b) CTL and TIP_nosh experiments, and (c) TIP_nosh and TIP experiments during 1985-2014. (d)-(f) are same as (a)-(c) but for NCRE at the TOA (W m^{-2}). Here, the dotting areas are over 99% significance level based on the Student's t-test. The solid black line denotes the TP's boundary over 3000m.

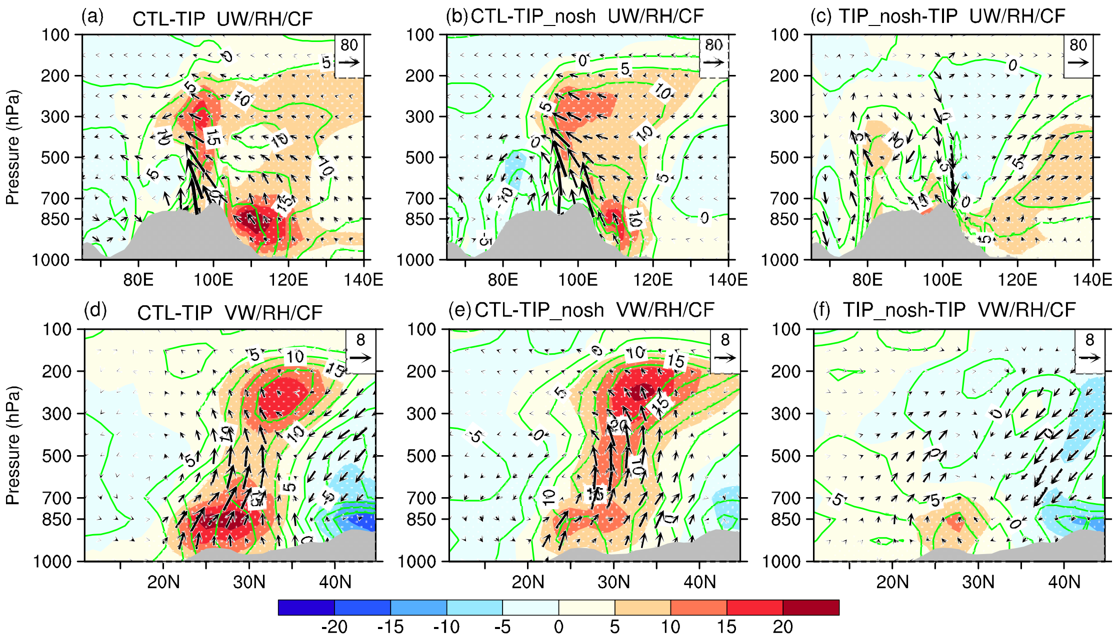

FIG. 7. March-April mean pressure-longitude cross section of cloud fraction (shading; CF: %), relative humidity (contour; RH: %), and wind circulations (vector; vertical wind (multiplied by 1000) in Pa s^{-1} and zonal wind in m s^{-1}) for the difference of (a) CTL and TIP experiments, (b) CTL and TIP_nosh experiments, and (c) TIP_nosh and TIP experiments averaged over 22-32°N. (d)-(f) are for pressure-latitude cross section of cloud fraction (shading; CF: %), relative humidity (contour; RH: %), and wind circulations (vector; vertical wind (multiplied by 200) is in Pa s^{-1} and meridional wind (multiplied by 0.05) in m s^{-1}) averaged over 104-122°E. Here, the period is 1985-2014 and the gray shading is the orography altitude; the dotting areas are over 99% significance level based

on the Student's t-test for cloud fraction.

Here, the differences between the control and two orography-sensitive experiments are calculated to identify respective impacts from thermal, mechanical, and combined forcings of Asian large-scale orography. Figure 6 shows the geographical distribution of cloud amount and NCRE due to orography forcing. In the combined forcing experiment, cloud amount significantly increases by 10-30% from the TP to East China Sea while it decreases by 5-30% from Central Asia to North China compared with the control run (Fig. 6a). The changes over most of the afore-mentioned regions are over 99% significance level based on the Student's t-test. Due to both orography forcings, cloud radiative cooling at the TOA is also enhanced over the Bay of Bengal, SEC, and East China Sea (Fig. 6d). It is noteworthy that the cloud radiative cooling doesn't strengthen with the increase in cloud amount over the whole TP, and it even decreases over the eastern and western TP (Fig. 6d). This different behavior of cloud amount and CREs over the TP very likely results from vertical cloud distribution forced by the TP's topography, which is shown in Figs. 7, S7, and S8. When only the thermal forcing is introduced, increased cloud amount occurs from the central and eastern TP to South Japan while cloud amount is reduced over South Asia and South China Sea (Fig. 6b). Note that intensified cloud radiative cooling mainly appears over SEC (Fig. 6e). These changes in cloud amount and cloud radiative cooling due to the thermal forcing seem to be limited just around the TP, and its impact scope doesn't extend to ECO (Figs. 3c and 6b,e). When the mechanical forcing is considered alone, the spatial pattern of cloud amount and NCRE is similar to those in the combined forcing, especially in mid-high latitudes (Figs. 6c,f). Relative to the thermal and combined forcings, the center position of cloud amount and NCRE over SEC migrates southeastward over ocean areas in the mechanical forcing (Figs. 6b,c,e,f).

Figure 8 gives domain-mean changes in total cloud amount (TCF) and CREs due to large-scale orography forcing. Over SEC, the combined large-scale orography forcing increases TCF, NCRE, SWCRE, and LWCRE by 24%, −32.3 W m^{-2}, −39.6 W m^{-2}, and 7.3 W m^{-2}, respectively. Both thermal and mechanical forcings can increase TCF and cloud radiative cooling at the TOA. The thermal forcing contributes to 57.1% and 47.6% for TCF and NCRE over SEC, respectively, and the mechanical forcing accounts for 42.9% and 52.4% of the counterparts (Fig. 8a). Particularly, the increase in low cloud amount over SEC is mainly attributed to the thermal forcing (Figs. 7b,e). As a result, the primary contribution to SWCRE magnitude is thermal forcing, with a ratio of 63.6%. The thermal forcing enhances high cloud amounts over SEC while the mechanical forcing lightly reduces them (Fig. 7b). Thus, increased LWCRE over SEC is mainly from the thermal forcing. Due to the offset between LWCRE and SWCRE, the domain-mean changes in NCRE magnitude forced by the thermal and mechanical forcings are close over SEC (Fig. 8a). In the atmosphere, $SWCRE_A$ also increases because low clouds enhanced by both orography forcings can intensify atmospheric shortwave absorption while the mechanical forcing reduces $LWCRE_A$ because increased low clouds inhibit downward longwave radiation (Figs. 7a-c and 8a). The change in $NCRE_A$ due to the combined large-scale orography is thereby small over SEC (Fig. 8a).

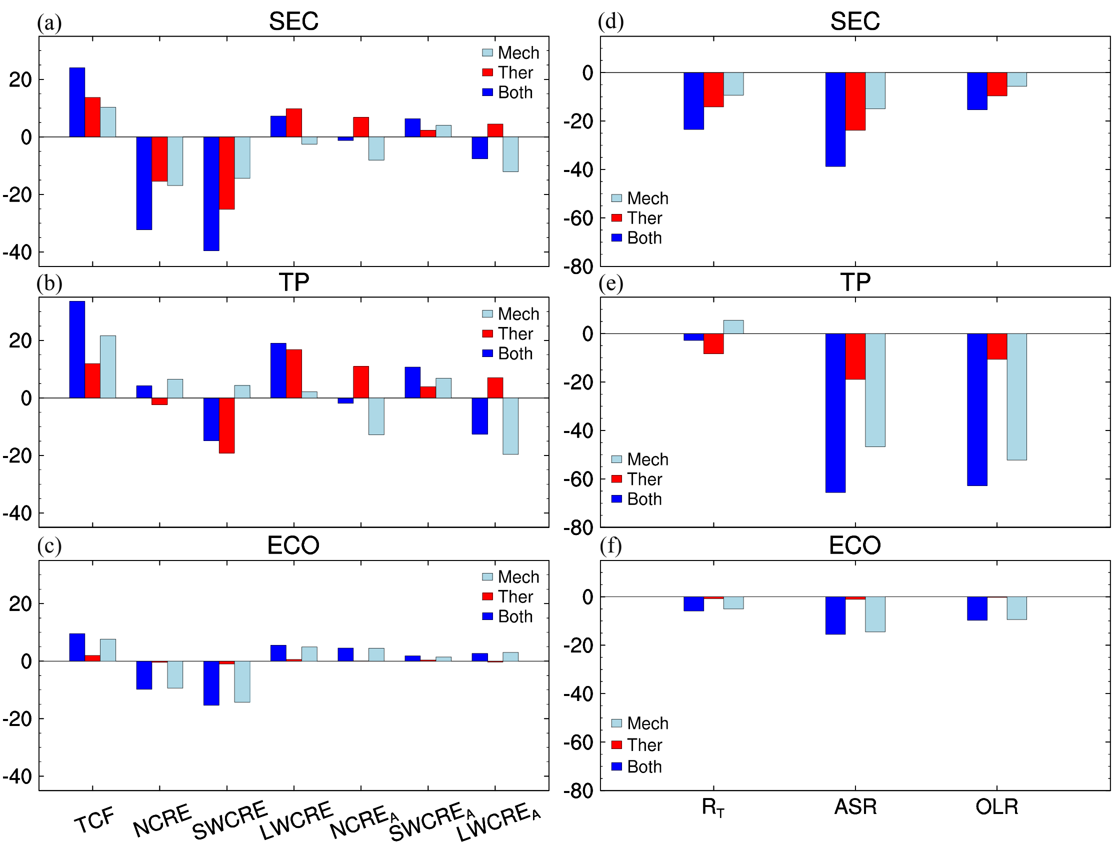

FIG. 8. March-April mean TCF (%) and CREs (W m^{-2}) induced by the thermal (red), mechanical (light blue), and combined (blue) effects of Asian large-scale orography averaged over (a) SEC, (b)

the TP, and (c) ECO. (d)-(f) are same as (a)-(c) but for radiation budget (W m^{-2}) at the TOA. Here, the data period is 1985-2014.

Over ECO, the noticeable point is that the mechanical forcing dominates the increases in TCF and CREs due to the combined forcing (Fig. 8c). For example, the increases in TCF and NCRE forced by the mechanical role are 7.6%, and −9.4 W m^{-2} averaged over ECO, respectively, which account for 79.4% and 95.8% of the combined forcing contribution, respectively (Fig. 8c). Relatively, the changes in TOA CREs are much more significant than atmospheric CREs over SEC and ECO, and their dominant items are SWCRE. Over the TP, the combined forcing increases TCF, SWCRE, and LWCRE by 33.6%, −14.8 W m^{-2}, and 19.0 W m^{-2}, respectively. The primary contribution to TCF arises from the mechanical forcing that accounts for 64.5% of the combined forcing (Fig. 8b). The differences in the changes in LWCRE and SWCRE resulting mainly from the thermal forcing are not large, but their signs are opposite, leading to a moderate decrease in NCRE in the combined orography forcing over the TP (Fig. 8b). Moreover, the changes in LWCRE and its atmospheric counterparts are larger over the TP than the other two regions. For example, the decreased $LWCRE_A$, with a value of −19.6 W m^{-2} averaged over the TP, is larger than the counterparts (−12.1 and 3.0 W m^{-2}) over SEC and ECO (Fig. 8). The larger change in $LWCRE_A$ over the TP relates to increased low-middle cloud amount caused by the mechanical forcing (Figs. 8b and S7c), which can weaken downward longwave radiation from the atmosphere. Here, these changes in atmospheric CREs demonstrate marked influences of Asian large-scale orography on the vertical distribution of cloud amounts over the TP, SEC, and adjacent Pacific regions.

The changes in R_T due to the combined orography forcing are −23.5, −5.9, and −2.8 W m^{-2} averaged over SEC, ECO, and the TP, respectively (Figs. 8d-f). Asian large-scale orography poses a TOA radiative cooling role over these regions. Over SEC, the primary effect is from the thermal forcing, with a 60.4% contribution to the change in magnitude of R_T (Fig. 8d). The thermal forcing decreases OLR due to low temperature at the top of increased low-middle clouds and also reduces ASR because of the cloud shortwave reflecting role. Over the TP, the decreased R_T primarily arises from the thermal forcing, with a change of −8.3 W m^{-2}, and is secondly from the mechanical forcing, with a change of 5.5 W m^{-2} (Fig. 8e). The mechanical forcing decreases ASR and OLR by −46.7 W m^{-2} and −52.2 W m^{-2}, respectively, and the counterparts by the thermal forcing are −18.9 W m^{-2} and −10.6 W m^{-2}, respectively (Fig. 8e). As mentioned above, the mechanical forcing significantly decreases surface temperature owing to the high TP elevation and thereby decreases OLR. When the high TP is excluded, the westerly and subtropical descent in the west of the TP position can move eastward, which reduces regional cloud amounts. In contrast, the climbing effect forced by the TP can increase cloud amounts over the western and central TP. Increased cloud amounts over the TP can reflect shortwave radiation and the mechanical forcing therefore reduces ASR over the TP. Similarly, the thermal forcing can also decrease ASR and OLR over the TP via increasing cloud amounts over the central and eastern TP (Figs. 6b, S7b), but the induced magnitude is much weaker than those by the mechanical forcing (Fig. 8e). Actually, the calculation method of R_T (the difference between ASR and OLR) makes the thermal forcing seem to be the dominant role of the R_T's change over the TP. As for the magnitude, the mechanical forcing is still the primary contributor to the change in ASR and OLR over the TP. Over ECO, the combined orography forcing can decrease R_T, ASR, and OLR, and the mechanical forcing contributes to 86.3%, 93.3%, and 97.4% of the magnitude changes in domain-mean R_T, ASR, and OLR, respectively (Fig. 8f). In contrast, the thermal forcing has a much weak contribution to the R_T's change over ECO. This further demonstrates that the thermal effects of Asian large-scale orography on cloud amount and R_T are limited in the TP's surrounding regions and are hard to reach farther places.

In short, Asian large-scale orography significantly intensifies cloud amount and cloud radiative cooling over SEC and ECO, but its thermal and mechanical forcings have different behaviors in the two regions. The thermal forcing enables the magnitude centers of low clouds and their radiative cooling to move westward torwards the eastern TP, with a peak position over SEC. The mechanical forcing pushes the distribution of cloud amounts southeastward over SEC and ECO.

5. Possible climatic mechanisms in the perspective of meteorological conditions

Cloud formation and distribution highly depend on ascending motion and water vapor supply (Roger and Rogers, 1989). Particularly, persistent spring ascending motion helps to generate and maintain low-middle clouds over East Asia, especially over SEC (Li et al., 2019). Hence, we focus on analyzing critical meteorological conditions induced by Asian large-scale orography's forcings.

a. The thermal forcing

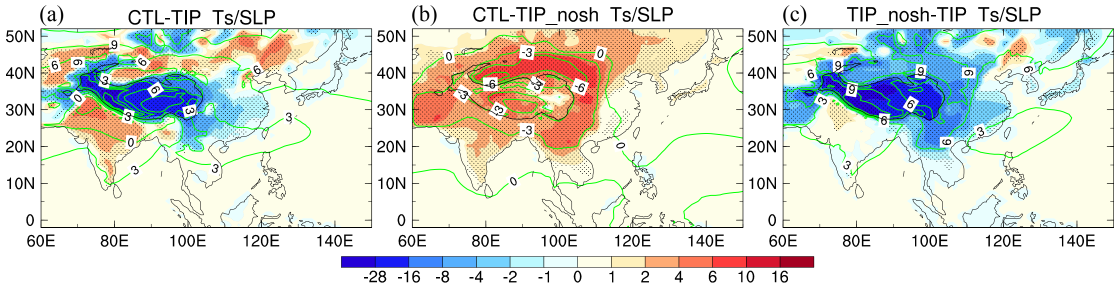

FIG. 9. March-April mean surface temperature (shading; Ts: K) and sea level pressure (contour; SLP: hPa d^{-1}) for the difference of (a) CTL and TIP experiments, (b) CTL and TIP_nosh experiments, and (c) TIP_nosh and TIP experiments during 1985-2014. The dotting areas are over 99% significance level based on the Student's t-test for surface temperature. The solid black line denotes the TP's boundary over 3000m.

Figure 9 presents the distribution of Ts and sea level pressure (SLP) induced by the orography forcing. When the thermal forcing is introduced alone, induced surface sensible heat generates an obvious surface warming (up to 6 K) over the TP, Yungui, and Mongolia Plateaus and Indian continents, with a cyclonic SLP anomaly (Fig. 9b). Thus, a low-level cyclonic flow as a circulation response is triggered surrounding the TP (Fig. 10h). Owing to the thermal forcing of large-scale orography, considerable amounts of water vapor are imported into SEC by the southwesterly along the Bay of Bengal and by the southerly from South China Sea (Fig. 11b). In the meantime, an obvious 200-hPa anticyclonic caused by the thermal forcing appears over North China and Mongolia, with a significant high-level divergence (Fig. 10b). These high- and low-level circulation anomalies very likely relate to sensible-heat-driven air pump (SHAP) effect caused by the TP's thermal forcing. In spring and summer, the intense TP's surface heat can reach the middle troposphere and works as an elevated SHAP. According to the theory of thermal adaptation (Hoskins, 1991; Wu et al., 2009), the atmosphere over the heating region at around 30°N is expected to trigger a cyclonic circulation in the lower troposphere and anticyclonic circulation in the upper troposphere. Meanwhile, an ascending motion tends to develop on the eastern side of the heating region. Thus, the TP's SHAP effect can induce a significant ascent from the central TP to central China (Fig. 10e). As shown in Figs. 7b and S7b, the air over the eastern TP and SEC is pumped from the surface to 300-hPa, where the atmospheric relative humidity increases accordingly because of the air uplift and intensified water vapor, favoring air condensation and the formation of clouds. Moreover, a 200-hPa divergence induced by the thermal forcing further intensifies regional ascent (Fig. 10b). Thus, the thermal forcing produces a secondary circulation over SEC between 20-40°N, with a strong ascending motion around 30°N (Fig. 7e). It is worth noting that most of increased cloud water content due to the thermal forcing, with a liquid phase, is mainly distributed in low-middle levels over SEC (Figs. 7b,e and S8b,e). These clouds can produce strong cloud reflecting and radiative cooling roles mentioned above. Due to the thermal forcing of large-scale orography, increased low-middle clouds over SEC cause strong SWCRE, while enhanced high clouds intensify LWCRE and $LWCRE_A$ over SEC and the eastern TP (Figs. 7 and 8). The aforementioned circulation conditions triggered by the thermal forcing persist in March-April, when the cloud distribution over SEC thereby stays stable, with a long lifetime. Note that more water vapor is imported into SEC relative to the eastern TP with thinner air and lower atmospheric water content (Wang et al., 2022). Thus, persistent low clouds with larger water content over SEC in March-April can reflect shortwave radiation and causes a stronger SWCRE response to the thermal forcing.

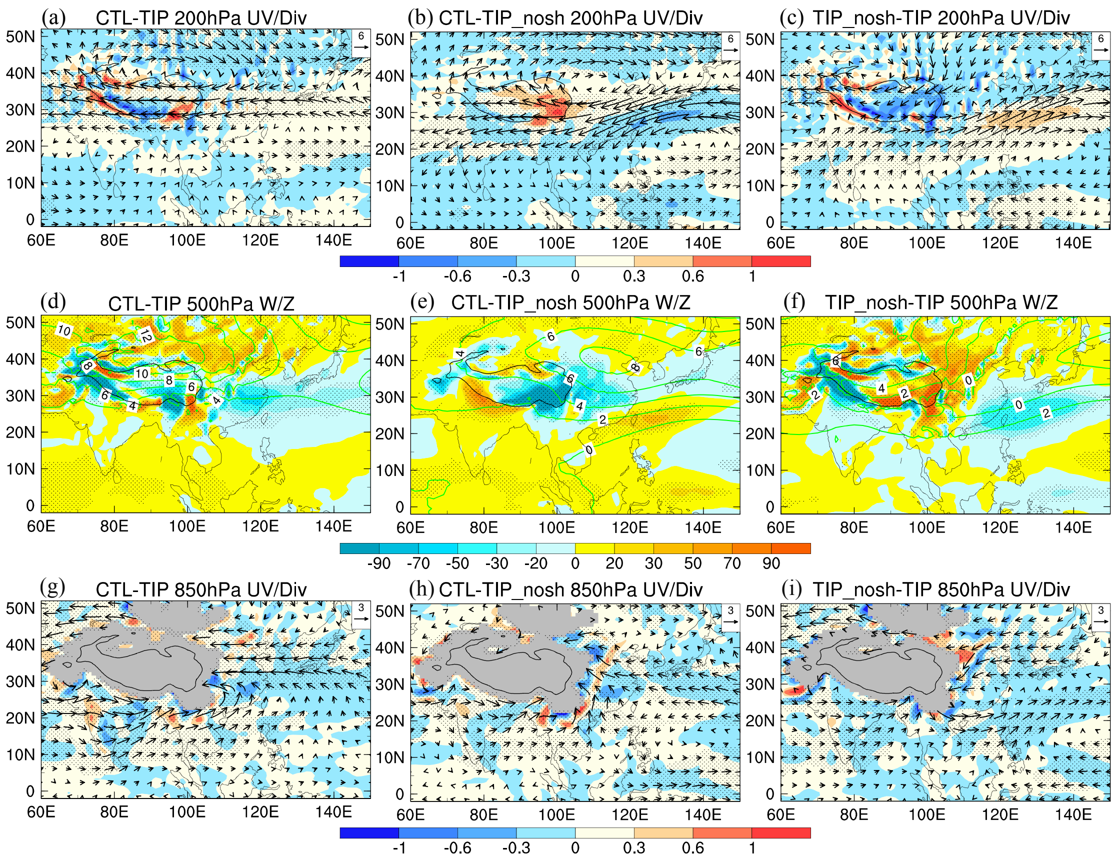

FIG. 10. March-April mean 200-hPa horizontal wind (vector; m s^{-1}) and divergence (shading; 10^5 s^{-1}) for the difference of (a) CTL and TIP experiments, (b) CTL and TIP_nosh experiments, and (c) TIP_nosh and TIP experiments during 1985-2014. (d)-(f) are 500-hPa vertical velocity (shading; hPa d^{-1}) and geopotential height (contour; 10 m) in these three runs. (g)-(i) are 850-hPa horizontal wind (vector; m s^{-1}) and divergence (shading; 10^5 s^{-1}) for the difference. The dotting areas are over 99% significance level based on the Student's t-test for 200-hPa divergence in (a)-(c), 500-hPa vertical velocity in (d)-(f), and 850-hPa divergence in (g)-(i), respectively. The solid black line denotes the TP's boundary over 3000m.

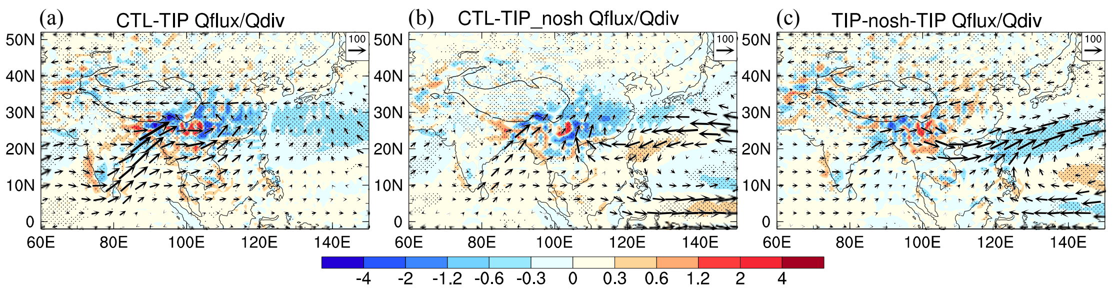

FIG. 11. March-April mean integrated column water vapor flux (vector; Qflux: kg m^{-1} s^{-1}) and divergence (shading; Qdiv: 10^4 kg m^{-2} s^{-1}) for the difference of (a) CTL and TIP experiments, (b) CTL and TIP_nosh experiments, and (c) TIP_nosh and TIP experiments during 1985-2014. The dotting areas are over 99% significance level based on the Student's t-test for column water vapor divergence. The solid black line denotes the TP's boundary over 3000m.

b. The mechanical forcing

When only the mechanical forcing is included, a strong surface cooling occurs over the TP and surrounding regions, accompanied by an anticyclonic SLP anomaly (Fig. 9c). The TP's surface cooling is caused by its high elevation that can lower air temperature via the lapse rate of surface air temperature. Because surface heat transport is excluded in the TIP_nosh run, it also contributes to significant surface cooling. However, surface cooling due to reduced surface sensible heating only accounts for a few degrees, whereas surface cooling owing to elevation increase can be more than 20 degrees for a lapse rate of 4 degrees per kilometer. In this regard, the mechanical forcing due to large-scale orography, especially the high TP elevation, will play a central role in the circulation responses over the Asian monsoon region. In the low-middle level, the TP acts as a physical obstacle in the eastern part of the Eurasian continent (Bolin, 1950; Yeh, 1957). The TP triggers a climbing effect and significant ascent along the western flank of the TP, while decent appears over the eastern side of the TP (Figs. 10f and S7c). Correspondingly, cloud amount increases over the western TP (Fig. 6c). Comparatively, ascent and increased cloud amounts induced by the thermal forcing occur over the eastern TP and its east (Figs. 10e and S7b). The TP's blocking role can directly weaken the low-level current over SEC while the TP's deflecting effect can increase the westerly from South China Sea to ECO (Fig. 10i). A low-level convergence and high-level divergence appear over eastern SEC and ECO, with an obvious 500-hPa ascending motion (Figs. 10c,f,i). As a result, low-middle level relative humidity and cloud amounts increase over eastern SEC and ECO (Fig. 7c). Over SEC, increased cloud amounts and cloud water content are mainly distributed in the low-level atmosphere because of the mechanical forcing, and thereby regional SWCRE is intensified (Figs. 7f, 8c, and S8c).

c. Comparison between the thermal and mechanical forcings

The horizontal and vertical distribution of cloud (amount and water content) and low-level circulation in the combined orography forcing are very similar to those in the thermal forcing over SEC (Figs. 7, 10, and S8). This demonstrates that a significant low-middle level ascent over SEC is primarily caused by the thermal forcing of Asian large-scale orography. The thermal forcing drives surface heating and cyclonic circulation surrounding the TP and pumps low-level air from the eastern TP and SEC. On the one hand, these triggered circulation conditions can produce considerable amounts of low and high clouds via ascent and air condensation. On the other hand, the ascent due to the TP's SHAP effect makes low-middle clouds migrate westward towards the TP, leading to a strong cloud radiative cooling center over SEC in March-April. Note that low- and high-level cloud amounts increase simultaneously over SEC, and SWCRE and LWCRE offset each other, leading to a moderately strengthened NCRE (Figs. 5d and 7a). The mechanical forcing secondarily contributes to low clouds and resultant cloud radiative cooling over SEC. The relative contribution of the two orography forcings is also shown in their relationships between vertical velocity and TCF over SEC. As for the thermal forcing, low-middle level velocity ascent prevails over SEC and relates well with TCF, with a correlation coefficient of −0.76 (Fig. 12a). In contrast, low-middle level vertical velocity has a very low correlation with TCF in the mechanical forcing (Fig. 12a).

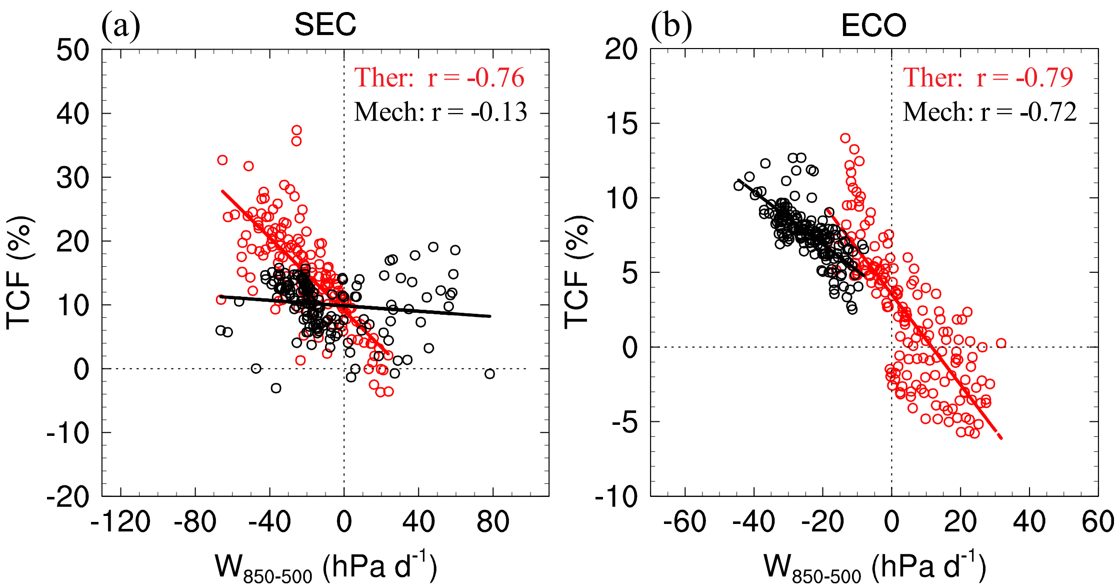

FIG. 12. Scatter plot of TCF (%) and vertical velocity (hPa d^{-1}) averaged between 850 and 500 hPa over (a) SEC (22-32°N, 104–122°E) and (b) ECO (22-32°N, 104–122°E). Here, red dots denote the results from the thermal forcing (CTL minus CTL_TIP_nosh) and red lines are the linear regression lines. Black colors are the counterparts from the mechanical forcing (TIP_nosh minus TIP). The correlation coefficients are marked with numbers at the top right-hand corner in (a) and (b). Here, the period is 1985-2014.

As shown in Figs. 6c and 6f, the distributions of cloud amount and NCRE in the combined forcing are close to the mechanical forcing over ECO. This indicates that the TP's mechanical deflecting effect primarily accounts for cloud amount and cloud radiative effect over ECO closely next to SEC. Over ECO, ascent relates well with TCF, with a correlation efficient of −0.72 for the mechanical forcing (Fig. 12b). Although the counterpart (−0.79) due to the thermal forcing is also high, low-high level circulation pattern and ascent forced by the mechanical effect are more consistent with enhanced cloud amount over ECO (Figs. 7c, S4c, 10c,f,i, and 11f). In addition, the responses of circulation and cloud amount to the combined orography forcing are similar to those in the mechanical forcing at Asian mid-high latitudes, including North China and Mongolia. For example, increased middle-level ascent over 20-25°N and descent around 35-40°N over East China primarily result from the mechanical forcing (Figs. 7d,f). These circulation variations are likely associated with the high-level jet changes that are strongly modulated by the TP's high elevation (Molnar et al., 2010). In TIP_nosh run, the mechanical forcing accelerates flow south of the TP, SEC, and ECO compared with TIP run (Figs. S3d,3f). Thus, a meridional circulation transverse to the jet axis is somewhat intensified, with ascent south of the jet and descent north of the jet (Liang and Wang, 1998), which provides a favorable dynamic background for increased (decreased) cloud amount over the south of SEC (North China and Mongolia) (Figs. 7c and 10c). Besides, large-scale meridional circulation dynamics may change with a westerly jet over East Asia. In TIP run, the subtropical descent region extends from the west of the TP to its east, and the Pacific subtropical anticyclone moves eastward relative to TIP_nosh run (Fig. S3). So, the meridional circulation responses induced by the TP forcing may be essential to vertical motion for cloud formation over SEC, ECO, and North China.

6. Conclusions and discussion

This study investigates the thermal and mechanical effects of Asian large-scale orography on spring cloud amount and atmospheric radiation budget over East Asia using CMIP6 GMMIP numerical experiments. In current orography, large amounts of low-middle clouds and strong cloud radiative cooling, with the global largest value up to −90.0 W m^{-2}, persist over SEC during March-April. This unique climatological feature is closely linked to Asian large-scale orography's forcing, especially the TP. The existence of Asian large-scale orography significantly increases spring cloud amounts and cloud radiative cooling over SEC and its eastward ocean, but the thermal and mechanical forcings of Asian large-scale orography have different contributions. The thermal forcing drives a significant surface heating and a low-level cyclonic flow over the TP and adjacent regions during March-April, and further pumps air from the low level to the middle troposphere via the TP's SHAP role. Meanwhile, the thermal forcing allows water vapor to be imported into SEC by the westerly from the south to the TP. Ascent and water vapor convergence triggered by the thermal forcing therefore helps to air condensation, low-middle clouds, and resultant strong spring cloud radiative cooling over SEC (Fig. 13). For example, low-middle level ascent caused by the thermal forcing relates well with TCF over SEC, with a correlation coefficient of −0.76. Moreover, this thermal forcing enables the position of low clouds and its radiative cooling to move westward towards the TP, with a magnitude center over SEC. The thermal effect contributes to 57.1%, 63.6%, 47.6%, and 60.4% of the changes in TCF, SWCRE, NCRE, and R_T due to Asian large-scale orography forcing over SEC, respectively. Therefore, the thermal effect of Asian large-scale orography is the primary contributor to cloud amount and TOA radiative cooling over SEC.

The TP's blocking role can weaken low-level westerly over SEC, while the TP's deflecting effect can increase the downstream high-level westerly, causing a low-level convergence and high-level divergence over eastern SEC and adjacent ECO. These induced circulation conditions provide a background for regional cloud formation over East Asia. Thus, the TP's mechanical forcing partly contributes to the cloud amount and TOA radiative cooling over SEC but primarily accounts for the counterparts over ECO. The mechanical forcing accounts for 79.4% of TCF, 93.3% of SWCRE, 95.8% of NCRE, and 86.3% of R_T over ECO for the combined contributions of Asian large-scale orography. Besides, the TP's climbing role can produce ascent and increased cloud amounts over the western and central TP. Notably, the TP's high elevation significantly decreases the surface temperature and thereby highly reduces OLR. These climatic processes are summarized in Fig. 13.

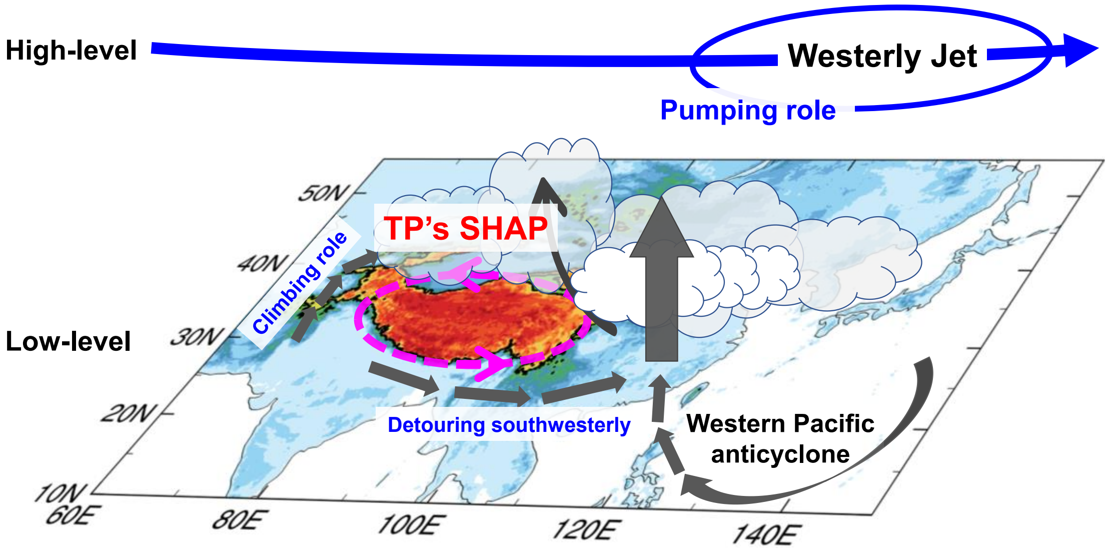

FIG. 13. Schematic diagram of Asian large-scale orography forcing on spring cloud amount over East Asia. Here, "SHAP" represents sensible-heat-driven air pump. The pink circle over the TP denotes the cyclone flow induced by the TP's thermal forcing. The narrow black arrows denote low-level currents induced by large-scale orography forcing. The wide vertical arrow denotes the low-middle level ascent, and the crooked arrow is for the ascent related to the TP's SHAP effect. The high-level blue circle denotes the westerly jet core with a pumping role for the air below. The white clouds over Southeast China denote clouds with strong shortwave reflecting cooling, while other clouds with light grey colors have moderate radiative cooling.

Our results indicate that the mechanical influences of Asian large-scale orography on downstream cloud and radiation budget are mainly from the TP because of its prominent higher elevation relative to its surroundings. As for the thermal forcing, Liu et al. (2017) suggested that the TP's sensible heat contributes more than twice that of the Iran Plateau and the TP plays a central role in regulating water vapor transport in the Asian subtropical monsoon region. Moreover, the induced surface heat and low-level cyclone can reach the Mongolia plateau and North China (Figs. 9b and 10h), where the land-atmosphere interaction is critical to East Asian climate (Cheng et al., 2019). In this sense, some thermal effects summarized above are probably linked to the Mongolia plateau. On geologic timescales, the mechanical forcing may be more prominent with the uplift of the TP, the substantial effects of which on the Asian climate have been supported by geological proxies and numerical simulations (Manabe and Broccoli, 1990; An et al., 2001). In recent decades, the TP is experiencing significant surface warming, almost two times the global mean (Duan et al., 2016; You et al., 2021). The TP's thermal forcing very likely plays a vital role in downstream East Asian clouds and radiation budget on the interannual timescale. Thus, Asian large-scale orography not only shapes the contemporary geographical distribution of spring East Asian cloud amount and atmospheric radiation budget to a large extent but also influences their future changes, especially in global warming.

In this study, the thermal forcing seems to be limited over East Asian continents to many degrees and does not extend eastward or southward ocean regions. The GMMIP experiments emphasize the roles of large-scale orography in Asian monsoon regions using observational sea surface temperature. However, this kind of model run doesn't consider well the SST change. Kitoh (2004) suggested that the air-sea coupling is very important in regulating the interplay between the Pacific subtropical anticyclone and South Asian monsoon circulation south of the TP. Besides, CMIP6 GMMIP experiments only provide monthly cloud amounts and radiative fluxes, which are not enough to investigate large orography forcing on the subseasonal evolution of East Asian cloud-radiation features. Hence, further model experiments and more thermal-dynamic diagnoses are needed to explore Asian large-scale orography forcings, particularly the TP, on East Asian cloud-radiation characteristics and energy budget.

Acknowledgments

This work is funded by the Strategic Priority Research Program of the Chinese Academy of Sciences (XDB40000000), the National Science Foundation of China (42275026 and 41975109), and UK–China Research and Innovation Partnership Fund through the Met Office Climate Science for Service Partnership (CSSP) China as part of the Newton Fund. We acknowledge the providers of NASA CERES-EBAF satellite products, CMIP6 data, and the NCAR Command Language software (http://dx.doi.org/10.5065/D6WD3XH5).

Data Availability

ERA5 reanalysis data are openly available at locations cited in the reference section. Cloud amounts and radiative fluxes are available from NASA CERES-EBAF satellite products at https://ceres.larc.nasa.gov/. CMIP6 data are openly available from ESGF nodes (https://esgf-node.llnl.gov/search/cmip6/).

Appendix

TABLE A1. Abbreviations of variable names used in this study

Variable name	Physical meaning	Unit
TOA	Top of the atmosphere	None
ASR	TOA absorbed shortwave radiation	W m^{-2}
LWCRE	Longwave cloud radiation effect at the TOA	W m^{-2}
$LWCRE_A$	Longwave cloud radiation effect in the atmosphere	W m^{-2}
NCRE	Net cloud radiation effect at the TOA	W m^{-2}
$NCRE_A$	Net cloud radiation effect in the atmosphere	W m^{-2}
OLR	Outgoing longwave radiation flux at the TOA under all-sky condition	W m^{-2}
OLRCS	Outgoing longwave radiation flux at the TOA under clear-sky condition	W m^{-2}
RSDT	Downward shortwave radiation flux at the TOA	W m^{-2}
RSUT	Outgoing shortwave radiation flux at the TOA under all-sky condition	W m^{-2}
RSUTCS	Outgoing shortwave radiation flux at the TOA under clear-sky condition	W m^{-2}
R_T	Radiation budget (equal to net radiative flux) at the TOA	W m^{-2}
SLP	Sea level pressure	Pa
SWCRE	Shortwave cloud radiation effect at the TOA	W m^{-2}
$SWCRE_A$	Shortwave cloud radiation effect in the atmosphere	W m^{-2}
TCF	Total cloud fraction	%
Ts	Surface temperature	K or ℃
ECO	East China Ocean	None
SEC	Southeast China	None
TP	Tibetan Plateau	None

Text: Formulas of cloud radiative effects

Cloud radiative effects (CREs) are widely used variables for effectively describing the bulk cloud effects on air-surface systems (Ramanathan et al. 1989; Allan et al. 2011). TOA CREs are defined as differences in TOA radiative fluxes between clear-sky and all-sky conditions:

$$\mathrm{LWCRE} = \mathrm{OLRCS} - \mathrm{OLR}, \quad (1)$$

$$\mathrm{SWCRE} = \mathrm{RSUTCS} - \mathrm{RSUT}, \quad (2)$$

$$\mathrm{LWCRE}_S = \mathrm{RLDS} - \mathrm{RLDSCS} - \mathrm{RLUS} + \mathrm{RLUSCS}, \quad (3)$$

$$\mathrm{SWCRE}_S = \mathrm{RSDS} - \mathrm{RSDSCS} - \mathrm{RSUS} + \mathrm{RSUSCS}, \quad (4)$$

$$\mathrm{LWCRE}_A = \mathrm{LWCRE} - \mathrm{LWCRE}_S, \quad (5)$$

$$\mathrm{SWCRE}_A = \mathrm{SWCRE} - \mathrm{SWCRE}_S, \quad (6)$$

$$\mathrm{NCRE} = \mathrm{LWCRE} + \mathrm{SWCRE}, \quad (7)$$

$$\mathrm{NCRE}_A = \mathrm{LWCRE}_A + \mathrm{SWCRE}_A, \quad (8)$$

where OLRCS and OLR are outgoing longwave radiation at the TOA under clear-sky and all-sky conditions, respectively; RSUTCS and RSUT are the corresponding outgoing SW radiative fluxes; RLDS and RLDSCS are downward longwave radiation at the surface under clear-sky and all-sky conditions, respectively, and RSDS and RSDSCS are the shortwave counterparts. RLUS and RLUSCS are upward longwave radiation at the surface under clear-sky and all-sky conditions, respectively, and RSUS and RSUSCS are the shortwave counterparts. Net CRE (NCRE) is the arithmetic sum of LWCRE and SWCRE. The subscripts "A" and "S" denote the atmosphere and surface, respectively.

References

Allan, R. P., 2011: Combining satellite data and models to estimate cloud radiative effect at the surface and in the atmosphere. Meteorological Applications, **18(3)**, 324–333.

An, Z., J. Kutzbach, W. Prell, and S. Porter, 2001: Evolution of Asian monsoons and phased uplift of the Himalaya-Tibetan plateau since Late Miocene times. *Nature*, 411, 62–66.

Bolin, B., 1950: On the influence of the Earth's orography on the general character of the westerlies. *Tellus*, 2, 184–195, https://doi.org/10.3402/tellusa.v2i3.8547.

Bony, S., B. Stevens, D. M. W. Friersonand, et al., 2015: Clouds, circulation and climate sensitivity. *Nat. Geosci.*, **8**, 261–268.

Boos, W. R., and Z. Kuang, 2010: Dominant control of the South Asian monsoon by orographic insulation versus plateau heating. *Nature*, **463(7278)**, 218–222.

Cess, R. D., G. L. Potter, J. P. Blanchet, et al. 1990: Intercomparison and interpretation of climate feedback processes in 19 atmospheric general circulation models. *J. Geophys. Res.*, 95(D10):16601–16615. doi:10.1029/JD095iD10p16601.

Chen H., W. Zhang, B. Zhou, F. Teng, J. Zhang, and Y. Zhou. 2019: Impact of nonuniform land surface warming on summer anomalous extratropical cyclone activity over East Asia. *J. Geophys. Res.-Atmos.*, **124(19)**:10306–10320. doi:10.1029/2018JD030165.

Chiang, J. C. H., W. Kong, C. H. Wu, and D. S. Battisti, 2020: Origins of East Asian Summer Monsoon Seasonality. *J. Climate*, **33(18)**, 7945–7965.

Ding, Y., and J. C. Chan, 2005: The East Asian summer monsoon: An overview. *Meteor. Atmos. Phys.*, **89(1–4)**, 117–142.

Duan, A. M., D. Hu, W. T. Hu, and P. Zhang, 2020: Precursor Effect of the Tibetan Plateau Heating Anomaly on the Seasonal March of the East Asian Summer Monsoon Precipitation. *J. Geophys. Res-Atmos.*, **125**, e2020JD032948.

Duan, A. M., Z. X, Xiao, and G. X. Wu, 2016: Characteristics of climate change over the Tibetan Plateau under the global warming during 1979–2014. *Clim. Change Res.*, **12(5)**, 374–381.

Duan, A., Li, F., Wang, M., Wu, G., 2011. Persistent weakening trend in the spring sensible heat source over the Tibetan Plateau and its impact on the Asian summer monsoon. *J. Clim*. 24, 5671–5682.

Eyring, V., S. Bony, G. A. Meehl, C. A. Senior, B. Stevens, R. J. Stouffer, and K. E. Taylor, 2016: Overview of the Coupled Model Intercomparison Project Phase 6 (CMIP6) experimental design and organization. *Geosci. Model Dev.*, **9**, 1937–1958.

Fasullo J. T., and K. E. Trenberth, 2008: The annual cycle of the energy budget. Part I: global mean and land-ocean exchanges. *J. Climate,* **21(10)**, 2297–2312.

Flato, G., Marotzke, J., Abiodun, B., Braconnot, P., Chou, S. C., Collins, W., Cox, P., Driouech, F., Emori, S., Eyring, V., Forest, C., Gleckler, P., Guilyardi, E., Jakob, C., Kattsov, V., Reason C., & Rummukainen, M. 2013: Evaluation of Climate Models. In: Climate Change 2013: The Physical Science Basis. Contribution of Working Group I to the Fifth Assessment Report of the Intergovernmental Panel on Climate Change [Stocker, T. F., Qin, D., Plattner, G.-K., Tignor, M., Allen, S. K., Boschung, J., Nauels, A., Xia, Y., Bex, V. & Midgley, P. M. (eds.)]. Cambridge University Press, Cambridge, United Kingdom and New York, NY, USA.

Flohn, H., 1957: Large-scale aspects of the "summer monsoon" in South and East Asia. *J. Meteor. Soc. Japan*, **35**, 180–186.

Forster, P., T. Storelvmo, K. Armour, W. Collins, J.-L. Dufresne, D. Frame, D.J. Lunt, T. Mauritsen, M.D. Palmer, M. Watanabe, M. Wild, and H. Zhang, 2021: The Earth's Energy Budget, Climate Feedbacks, and Climate Sensitivity. In Climate Change 2021: The Physical Science Basis. Contribution of Working Group I to the Sixth Assessment Report of the Intergovernmental Panel on Climate Change [Masson-Delmotte, V., P. Zhai, A. Pirani, S.L. Connors, C. Péan, S. Berger, N.

Caud, Y. Chen, L. Goldfarb, M.I. Gomis, M. Huang, K. Leitzell, E. Lonnoy, J.B.R. Matthews, T.K. Maycock, T. Waterfield, O. Yelekçi, R. Yu, and B. Zhou (eds.)]. Cambridge University Press, Cambridge, United Kingdom and New York, NY, USA, pp. 923–1054, doi:10.1017/9781009157896.009.

Guo, Z., T. Zhou, M. Wang, and Y. Qian, 2015: Impact of cloud radiative heating on East Asian summer monsoon circulation. *Environ. Res. Lett.*, **10**, 074014.

He, C., Wang, Z., Zhou, T., Li, T., 2019. Enhanced latent heating over the Tibetan Plateau as a key to the enhanced East Asian summer monsoon circulation under a warming climate. *J. Clim.*, 32, 3373–3388.

He, J. H., P. Zhao, C. W. Zhu, R. H. Zhang, and X. Tang, 2008: Discussions on the East Asian subtropical monsoon. *Acta Meteor. Sin.*, **66(5)**, 683–696.

Hersbach, H., B. Bell, P. Berrisford, S. Hirahara, A. Horanyi, J. Munoz-Sabater, and J. Thepaut, et al. 2020: The ERA5 global reanalysis. *Quart. J. Roy. Meteor. Soc.*, **146 (730)**, 1999–2049.

Hoskins, B. J. 1991: Towards a PV-Θ view of the general circulation. *Tellus*, **43AB**, 27–35.

Hu, Y., S. Rodier, K.-M. Xu, W. Sun, J. Huang, B. Lin, P. Zhai, D. Josset, 2010: Occurrence, liquid water content, and fraction of 498 supercooled water clouds from combined CALIOP/IIR/MODIS measurements. *J. Geophys. Res-Atmos.*, **115**, doi:10.1029/2009jd012384.

Hurrell, J. W., M. M. Holland, P. R. Gent, S. Ghan, J. E. Kay, P. J. Kushner, J.-F. Lamarque, W. G. Large, D. Lawrence, K. Lindsay, W. H. Lipscomb, M. C. Long, N. Mahowald, D. R. Marsh, R. B. Neale, P. Rasch, S. Vavrus, M. Vertenstein, D. Bader, W. D. Collins, J. J. Hack, J. Kiehl, and S. Marshall, 2013: The Community Earth System Model: A framework for collaborative research. *Bull. Amer. Meteor. Soc.*, **94**, 1339–1360. https://doi.org/10.1175/BAMS-D-12-00121.1.

Kiehl, J. T., and K. E.Trenberth, 1997: Earth's annual global mean energy budget. *Bull. Amer. Meteor. Soc.*, 78, 197–208.

Kiehl, J. T., 1994: On the observed near cancellation between longwave and shortwave cloud forcing in tropical regions. *J. Climate*, **7**, 559–565

Kitoh, A., 2004: Effects of mountain uplift on East Asian summer climate investigated by a coupled atmosphere-ocean GCM. *J. Climate*, **17(4)**, 783–802.

Klein, S. A., and D. L. Hartmann, 1993: The Seasonal Cycle of Low Stratiform Clouds. *J. Climate*, **6**, 1587–1606.

Li, J., and R. Yu, 2014: Characteristics of cold season rainfall over the Yungui Plateau. *J. Climate Appl. Meteor.*, **53**, 1750–1759.

Li, J. D., Z. A. Sun, Y. M. Liu, Q. L. You, G. X. Chen, and Q. Bao, 2021: Top-of-Atmosphere Radiation Budget and Cloud Radiative Effects over the Tibetan Plateau and Adjacent Monsoon Regions from CMIP6 Simulations. *J. Geophys. Res-Atmos.*, **126**, e2020JD034345, doi: 10.1029/2020JD034345.

Li, J. D., W. C. Wang, J. Y. Mao, Z. Q. Wang, G. Zeng, and G. X. Chen, 2019: Persistent spring cloud shortwave radiative effect and the associated circulations over southeastern China. *J. Climate*, **32**, 3069–3087.

Li, J. D., W.-C. Wang, X. Dong, and J. Mao, 2017: Cloud-radiation-precipitation associations over the Asian monsoon region: an observational analysis. *Climate Dyn.*, **49**, 3237–3255.

Li, Y., and H. Gu, 2006: Relationship between middle stratiform clouds and large scale circulation over eastern China. *Geophys. Res. Lett.*, **33**, L09706, doi:10.1029/2005GL025615.

Li, Y., D. W. J. Thompson, and S. Bony, 2015: The influence of atmospheric cloud radiative effects on the large-scale atmospheric circulation. *J. Climate*, **28**, 7263–7278.

Liang, X.-Z., W.-C. Wang, 1998: Associations between China monsoon rainfall and tropospheric jets. *Q. J. R. Meteorol. Soc.*, **124**, 2597–2623.

Liu, Y. M., Wang, Z. Q., Zhuo, H. F., et al. 2017. Two types of summertime heating over Asian large-scale orography and excitation of potentia vorticity forcing. II: Sensible heating over Tibetan–Iranian Plateau. *Sci. China Earth Sci.*, **60 (4)**, 733–744, doi:10.1007/s11430-016-9016-3.

Liu, Z. Y., 813: Answer Wei Zhongli's letter on the way of teachers.

Luo, H. L., Z. Q. Wang, S. Yang, and W. Hua, 2022: Revisiting the impact of Asian large-scale orography on the summer precipitation in Northwest China and surrounding arid and semi-arid regions. *Climate Dyn.*, https://doi.org/10.1007/s00382-022-06301-5.

Loeb, N. G., D. R. Doelling, H. Wang, W. Su, C. Nguyen, J. G. Corbett, L. Liang, C. Mitrescu, F. G. Rose, and S. Kato, 2018: Clouds and the Earth’s Radiant Energy System (CERES) Energy Balanced and Filled (EBAF) Top-of-Atmosphere (TOA) Edition-4.0 Data Product. *J. Climate*, **31**, 895–918.

Matus, A. V., T. S. L'Ecuyer, 2017: The role of cloud phase in Earth's radiation budget. *J. Geophys. Res-Atmos.*, **122**, 2559-2578, doi:10.1002/2016jd025951.

Molnar, P., W. R. Boos, and D. S. Battisti, 2010: Orographic Controls on Climate and Paleoclimate of Asia: Thermal and Mechanical Roles for the Tibetan Plateau. *Annu. Rev. Earth Pl. Sc.*, **38(1)**, 77–102.

Ramanathan, V. 1987: The role of earth radiative budget studies in climate and general circulation research. *J. Geophys. Res-Atmos.*, **92(D4)**, 4075–4095.

Rogers, R. R., and M. K. Yau, 1989: A Short Couse in Cloud Physics. Butterworth-Heinemann, 304 pp.

Rodwell, M. J., and B. J. Hoskins, 2001: Subtropical anticyclones and summer monsoons. *J. Climate*, **14**, 3192–3211.

Stephens, G. L., 2005: Cloud feedbacks in the climate system: A critical review. *J. Climate*, **18(2)**, 237–273.

Sun, H., and X. Liu, 2021: Impacts of dynamic and thermal forcing by the Tibetan Plateau on the precipitation distribution in the Asian arid and monsoon regions, *Climate Dyn.*, **56(7-8)**, 2339–2358.

Wang, Q., H. Zhang, S. Yang, Q. Chen, X. Zhou, B. Xie, Y. Wang, G. Shi, and M. Wild, 2022: An assessment of land energy balance over East Asia from multiple lines and the roles of Tibet Plateau, aerosols, and clouds. *Atmos. Chem. Phys.*, 22, https://doi.org/10.5194/acp-22-15867-2022

Wan, R. J., and G. X. Wu, 2007: Mechanism of the spring persistent rains over southeastern China. *Sci. China Ser. D: Earth Sci.*, **50**, 130–144.

Wild, M., 2020: The global energy balance as represented in CMIP6 climate models. *Climate Dyn.*, **55 (3)**, 553–577.

Wu, C.-H., and M.-D. Chou, 2013: Tibetan Plateau westerly forcing on the cloud amount over Sichuan Basin and the early Asian summer monsoon. *J. Geophys. Res-Atmos.*, **118(14)**, 7558–7568.

Wu, G., Y. Liu, B. He, Q. Bao, A. Duan, and F. F. Jin, 2012: Thermal controls on the Asian summer monsoon. *Sci. Rep.*, **2**, 404.

Wu, G. X., A. M. Duan, Y. M. Liu, J. Y. Mao, R. C. Ren, Q. Bao, B. He, B. Q. Liu, and W. T. Hu, 2015: Tibetan Plateau climate dynamics: recent research progress and outlook. *Natl. Sci. Rev.*, **2(1)**, 100–116.

Wu, G. X., Y. Liu, X. Zhu, W. Li, R. Ren, A. Duan, and X. Liang, 2009: Multi-scale forcing and the formation of subtropical desert and monsoon. *Annales Geophysicae-Germany*, **27(9)**, 3631–3644.

Wu, G. X., Y. M. Liu, T. M. Wang, R. J. Wan, X. Liu, W. P. Li, Z. Z. Wang, Q. Zhang, A. M. Duan, X. Y. Liang, 2007: The influence of mechanical and thermal forcing by the Tibetan Plateau on Asian climate. *J. Hydrometeor.*, **8(4)**, 770–789.

Wong, K. C., S. Liu, A. G. Turner, and R. K. Schiemann, 2018: Different Asian Monsoon Rainfall Responses to Idealized Orography Sensitivity Experiments in the HadGEM3-GA6 and FGOALS-FAMIL Global Climate Models. *Adv. Atmos. Sci.*, **35(8)**, 1049–1062.

Song Y, Li X, Bao Y, Song Z, Wei M, Shu Q, Yang X (2020) FIO-ESM v2.0 outputs for the CMIP6 Global Monsoons Model Intercomparison Project experiments. *Adv. Atmos. Sci.*, **37(10)**, 1045–1056.

Yanai, M., and G. X. Wu, 2006: Effects of the Tibetan Plateau. The Asian Monsoon, B. Wang et al., Eds., Springer, 513–549.

Yanai, M., C. Li, and Z. Song, 1992: Seasonal heating of the Tibetan Plateau and its effects on the evolution of the Asian summer monsoon. *Quart. J. Roy. Meteor. Soc.*, **70**, 319–351.

Yeh, T. C., S. W. Lo, and P. C. Chu, 1957: The wind structure and heat balance in the lower troposphere over Tibetan Plateau and its surrounding. *Acta Meteor. Sin.*, **28**, 108–121, https://doi.org/10.11676/qxxb1957.010.

Ying, B., Z. Song, F. Qiao, 2020: FIO- ESM version 2.0: Model description and evaluation. *J. Geophys. Res-Ocean*, **125(6)**, e2019JC016036.

You, Q. L., Cai, Z., Pepin, N., Chen, D., Ahrens, B., Jiang, Z.,Wu, F., Kang, S., Zhang, R, Wu, T., Wang, P, Li, M., Zuo, Z., Gao, Y., Zhai, P., & Zhang, Y. et al. (2021), Warming amplification over the Arctic Pole and Third Pole: Trends, mechanisms and consequences. *Earth-Science Reviews*, **217**, 103625.

Yu, R. C., B. Wang, and T. J. Zhou, 2004: Climate effects of the deep continental stratus clouds generated by the Tibetan Plateau. *J. Climate*, **17**, 2702–2713.

Yu, T. T., Chen, W., Gong, H. N., Feng, J., Chen, S. F., Shangfeng Chen, 2022: Comparisons between CMIP5 and CMIP6 models in simulations of the climatology and interannual variability of the east asian summer Monsoon. *Climate Dyn.*, https://doi.org/10.1007/s00382-022-06408-9.

Zelinka, M. D., T. A. Myers, D. T. Mccoy, S. Po-Chedley, P. M. Caldwell, P. Ceppi, S. A. Klein, and K. E. Taylor, 2020: Causes of Higher Climate Sensitivity in CMIP6 Models. *Geophys. Res. Lett.*, **47**, e2019GL085782.

Zhang, Y., R. Yu, J. Li, W. Yuan, and M. Zhang, 2013: Dynamic and Thermodynamic Relations of Distinctive Stratus Clouds on the Lee Side of the Tibetan Plateau in the Cold Season. *J. Climate*, **26**, 8378–8391.

Zhao, P., R. Zhang, J. Liu, X. Zhou, and J. He, 2007: Onset of southwesterly wind over eastern China and associated atmospheric circulation and rainfall. *Climate Dyn.*, **28**, 797–811.

Zhou, T., and Coauthors, 2016: GMMIP (v1.0) contribution to CMIP6: Global Monsoons Model Inter-comparison Project. *Geosci. Model Dev.*, **9**, 3589–3604.